Journal of The Electrochemical Society, **157** (1) D16-D20 (2010)
0013-4651/2009/157(1)/D16/5/$28.00 © The Electrochemical Society

Structure, Electrical Properties, and Surface Reactivity of CVD-Made Functional Complex Oxides

Naoufal Bahlawane,[z]
Patrick Herve Tchoua Ngamou, and Katharina Kohse-Höinghaus

Department of Chemistry, Bielefeld University, 33615 Bielefeld, Germany

The growth of pure-phase perovskites and spinels is reported using pulsed-spray evaporation chemical vapor deposition (CVD). Besides the near-bulk properties of 250 nm thick perovskites, an unusual surface confinement of charge transport was observed in ultrathin, <10 nm, polycrystalline $LaCoO_3$ films, resulting in an electrical resistivity that appears to be lower than that of a single crystal. Using doping strategy as a tool to tune the physicochemical properties of the spinel structure of cobalt oxide was demonstrated, enabling the establishment of direct correlations between its properties and catalytic activity. Iron doping of Co_3O_4 has enabled the control of the reducibility of the spinel with direct consequences on the catalytic oxidation of CO and the control of the abundance of basic adsorption sites, which affected the catalytic oxidation of ethanol.
 [DOI: 10.1149/1.3247543]

Manuscript submitted June 30, 2009; revised manuscript received September 17, 2009. Published November 3, 2009. This was Paper 2496 presented at the Vienna, Austria Meeting of the Society, October 4–9, 2009.

Oxides with spinel and perovskite structures are intensively investigated as materials for innovative technological developments using effects such as electronic and ionic conductivities, high temperature superconductivity, colossal magnetoresistance, colossal resistance switching, and multiferroicity.[1-7] The high defect tolerance of these structures makes them suitable materials for the chemical engineering to tailor their properties to specific applications.[8-10] Furthermore, the controlled growth of high quality thin and ultrathin films has enabled the combination of various functionalities and also the discovery of new phenomena[11,12] such as unusual charge states that are inaccessible in bulk materials. However, chemical vapor deposition (CVD) remains infrequently involved, which is presumably due to the difficulty in controlling the growth of a single phase of complex oxides and the handling of several precursors, although the liquid delivery process has allowed surmounting these difficulties in several cases.[13,14]

In the present study, we report a successful growth of several functional complex oxides as thin and ultrathin films using pulsed spray evaporation CVD. The size effect on the electrical charge transport and the doping effect on the catalytic reactivity were investigated to evidence the interplay between the composition, the properties, and the surface reactivity.

Experimental

The deposition of metal oxides was performed in a cold wall CVD reactor, which was operated at a pressure of 50 mbar. Metal acetylacetonates, purchased from STREM chemicals, were used to prepare liquid feedstock precursor solutions that have been delivered to the reactor using a home-built pulsed spray evaporator. The selection of metal acetylacetonates was encouraged by their solubility in ethanol, use as a solvent, and their stability in solution under ambient conditions. Furthermore, acetylacetonate complexes are readily available for several metals, which suppresses the inconvenience of eventual ligand exchange in a precursor solution containing more than one precursor. The pulsed delivery was carried out using an opening time of 2.5 ms and a controlled frequency from 4 to 14 Hz, enabling a feeding rate that attains 570 μL/min with a frequency of 14 Hz. The total metal concentration in the precursor feedstock was set at 5 mM, while the relative metal ratios were adjusted to obtain the desired material. The composition of the film usually diverges from that of the used liquid feedstock, but linear dependence was always observed. This behavior was mainly attributed to the contrasting sticking coefficient of the precursors, and the linear dependence between the feedstock and the film compositions was advantageously used for an accurate control of the composition of the films. The evaporation temperature, 180–220°C, was optimized to suppress the precursors' decomposition or condensation in the evaporation and transport parts of the reactor. Besides the liquid feedstock, 1 slm of oxygen and 0.5 slm of nitrogen were used, and the substrate, planar stainless steel, or glass was heated to deposition temperatures of 400–700°C.

The obtained films were characterized by X-ray diffraction (XRD, PHILIPS X'Pert) and Fourier transform infrared (FTIR) spectroscopy (Thermo Nicolet 5700) with a home-built emission cell that is described elsewhere.[15] The FTIR emission spectroscopy was used for film characterization and the monitoring of the reducibility in a temperature-programmed mode. The resistivity of the grown films, on glass or α-Al_2O_3-coated silicon substrates, was measured as a function of the temperature in ambient atmosphere using the standard computer-controlled dc four-probe equipment. The thickness of the grown films was obtained gravimetrically (Mettler ME30, digital resolution of 1 μg) and confirmed geometrically for the thickest films (scanning electron microscopy, S-450 Hitachi).

The reactivity of the obtained films was investigated using a home-built stainless steel cell that accommodates a single planar–circular glass sample with a diameter of 25 mm and a thickness of 0.3 mm and which occupies $\sim$30% of the inner volume in the catalytic cell. The residence time of the gas in the catalysis cell was estimated at 3 s with a total flow of 10 sccm as used in this study. The temperature of the catalytic bed was monitored using a thermocouple that is in contact with the surface of the sample, while the exhaust gas composition was monitored by FTIR using a home-built transmission cell.

Results and Discussion

The investigated complex oxides in this study are lanthanum-based transition metal oxides, which crystallize in the perovskite structure, and cobalt-oxide-based spinels. The challenging task in both cases is the attainment of a single phase of the targeted materials while retaining the possibility of tuning their compositions.

Perovskite oxide and thickness effect.— The growth of lanthanum-based perovskites was performed involving nickel, cobalt, iron, chromium, and manganese as transition metals. The major difficulty encountered in this study is the accurate control of the deposition parameters to suppress the formation of separate phases of lanthanum oxide or the oxide of the transition metal. The depicted XRD patterns in Fig. 1 show pure phases of the perovskite, the growth of which was optimized at deposition temperatures of 700–750°C. $LaCoO_3$, $LaCrO_3$, and $LaFeO_3$ crystallize in the cubic perovskite structure with the symmetry group $Pm3m$, whereas $LaMnO_3$ crystallizes in the rhombohedral structure (R-$3c$). All films

[z] E-mail: naoufal@pc1.uni-bielefeld.de

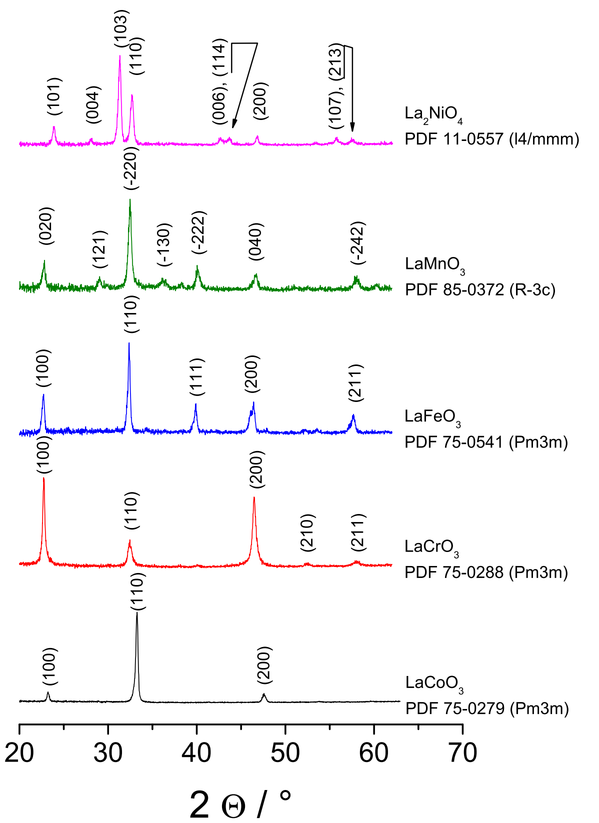

Figure 1. (Color online) XRD patterns of the grown perovskite thin films with the identification of the reflexes using the powder diffraction database.

exhibit random orientations except $LaCrO_3$, which shows a pronounced (100) orientation. The composition of the liquid feedstock in terms of the ratio $R = M(acac)_n/La(acac)_3$ was revealed to be the key control parameter. The growth of single-phase perovskites was attained with $R = 0.4$ for $LaFeO_3$ and $LaCoO_3$ and with $R = 1$ for $LaMnO_3$ and $LaCrO_3$. In contrast to other transition metals, nickel has a tendency to readily form the layered structure La_2NiO_4 of the K_2NiF_4 type. The crystallite size of all obtained films was calculated to be 50–70 nm, for films with a thickness of 250 nm, based on the broadening of the most intense diffraction peak.

The temperature-dependent electrical conductivity and the thermoelectric coefficient of the obtained $LaCoO_3$, $LaCrO_3$, $LaFeO_3$, and $LaMnO_3$ films with a thickness of 250 nm have been measured.[16] All these films were shown to exhibit a p-type semiconducting behavior, and the characteristic bandgap energies were comparable to those of the corresponding polycrystalline bulk material, which is an indication of the purity of the obtained films.

Further optimization has shown that some perovskites, $LaCoO_3$ and La_2NiO_4, can be grown at temperatures as low as 400°C. The obtained films at low temperature show a smoother morphology even though the crystallite size compares to that of films grown at high temperature. Optical characterization using UV/visible absorption spectroscopy indicates that $LaCoO_3$ films with a thickness exceeding 300 nm exhibit bandgap energies corresponding to that of a bulk polycrystalline material. This observation hints at the absence of amorphous contamination phases. Typical cross-sectional scanning electron micrographs (Fig. 2) show that films are composed of densely packed nanoparticles regardless of the deposition temperature. The films grown at high temperatures exhibit columnar stacking of the nanoparticles forming the films.

The electrical properties of thick perovskite films (300 nm), obtained at high temperatures, have been reported previously.[16] Based on electrical and thermoelectrical characterizations of various pure

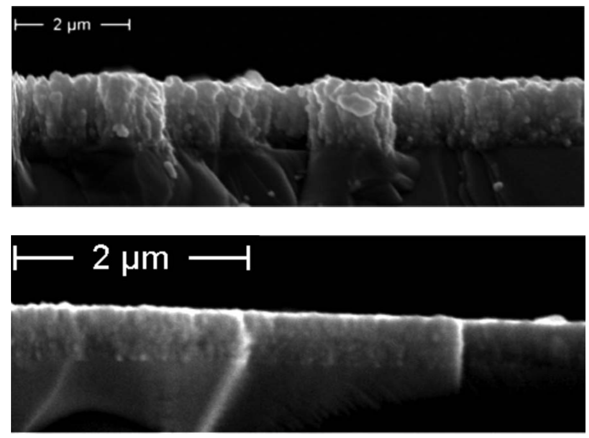

Figure 2. Cross-sectional scanning electron micrographs of grown $LaCoO_3$ films on silicon at 700°C (upper micrograph) and on glass at 400°C (lower micrograph).

perovskite thin films grown on α-Al_2O_3-coated silicon substrates, $LaCoO_3$ was revealed to possess the highest concentration and mobility of the charge carriers when compared to $LaMnO_3$, $LaCrO_3$, and $LaFeO_3$. Therefore, the study of the thickness effect on the electrical properties was performed here using $LaCoO_3$, which appears as a promising material.

The obtained $LaCoO_3$ films on glass substrates exhibit electrical conductivity at thicknesses as low as 2 nm, which hints at the coalescence of the films in the early stages of deposition. The systematic investigation of the electrical properties as a function of the thickness has drawn our attention to an unusual property of ultrathin films. As the crystallite size increases with the thickness of the films, the density of the grain boundaries decreases. Therefore, the resistivity (ρ) is expected to be higher for thinner films. As shown in Table I, an opposite trend is observed. What is even more striking is that films with thicknesses below 10 nm exhibit resistivities that are even lower than that of a bulk single-crystal $LaCoO_3$ (4–5 Ω cm) at 300 K,[17,18] which makes the use of resistivity as an intensive physical property questionable. The XRD patterns show that the diffraction angle of the reflex (110), presented in Fig. 3, is not influenced by the thickness of the film. Therefore, the calculated interplanar spacing is rather constant, as shown in Table I, which rules out the presence of interfacial strain or deviation from stoichiometry in the ultrathin films. The crystallite sizes calculated from the broadening of the XRD reflexes are larger than the thickness of films below 30 nm, which is an indication of the lateral growth of the crystals. This observation corroborates with the early stage coalescence of the films deduced from the electrical conductivity.

The investigation of the electrical resistivity as a function of the temperature (Fig. 4a) confirms the puzzling superior electrical con-

Table I. Structural and electrical properties of ultrathin $LaCoO_3$ films as a function of the thickness.

Thickness (nm)	d^a (Å)	Crystallite size (nm)	$\rho_{300\ K}$ (Ω cm)
2	—	—	0.66
8	2.723	37	2.38
30	2.721	49	16.66
70	2.722	54	25.58
100	2.723	60	36.60

[a] Lattice spacing between the (110) planes of the rhombohedral $LaCoO_3$ perovskite. Films with a thickness of 2 nm are inaccessible to grazing incidence X-ray diffraction analysis.

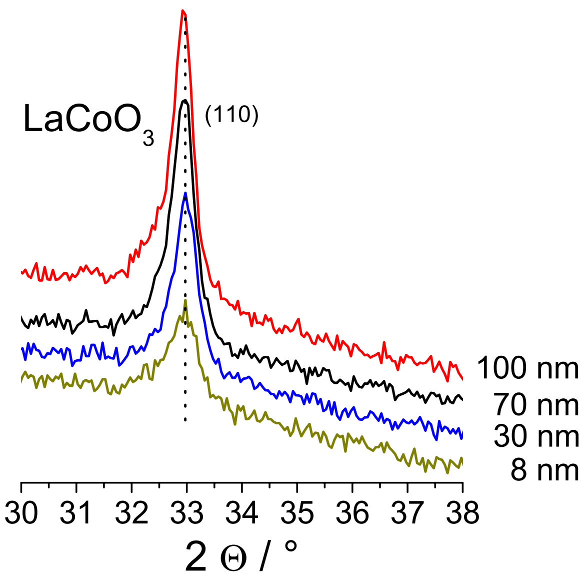

Figure 3. (Color online) XRD (110) reflex of $LaCoO_3$ as a function of the thickness for films obtained on glass at a temperature of 400°C.

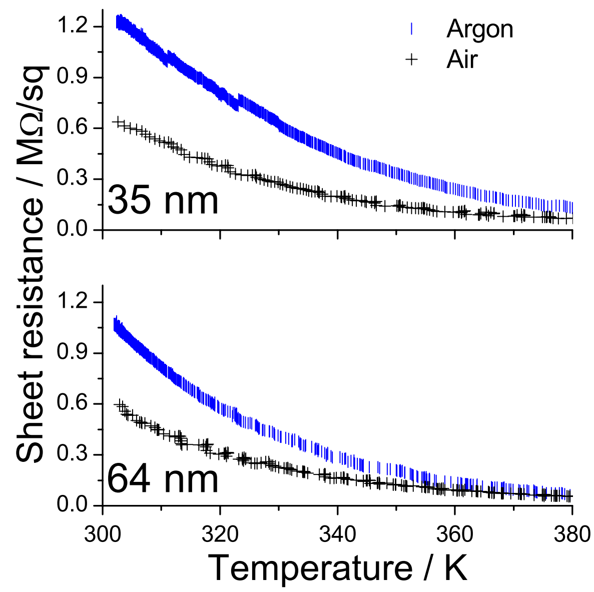

Figure 5. (Color online) The effect of oxygen desorption on the electrical sheet resistance of 35 and 64 nm thick $LaCoO_3$ films.

ductivity of thinner films if the involvement of the entire film in the charge transport is assumed. Nevertheless, the sheet resistance presented in Fig. 4b shows no thickness dependence. The sheet resistance (Ω/□) is an intensive property in the surface dimensions but

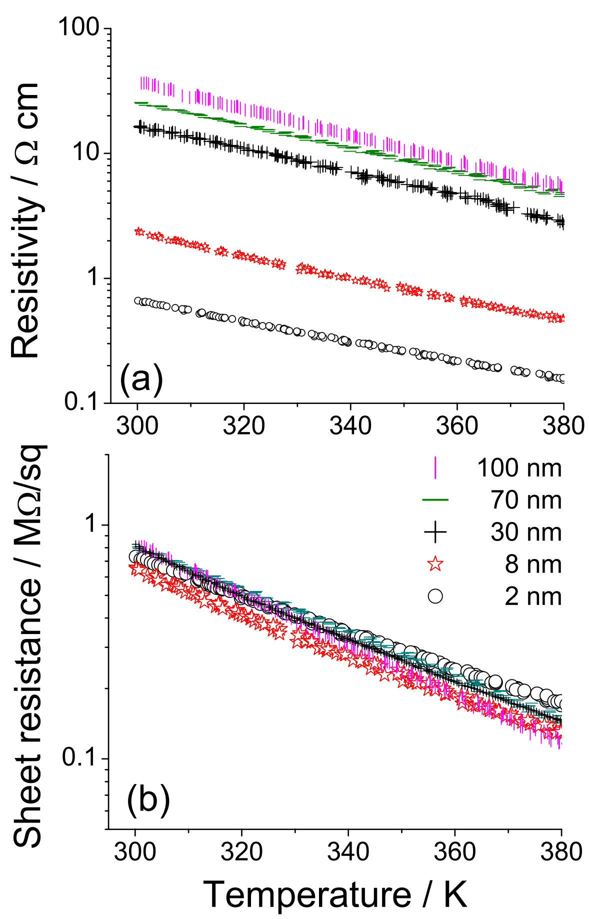

Figure 4. (Color online) (a) Temperature-dependent resistivity and (b) sheet resistance of $LaCoO_3$ thin films with various thicknesses.

is extensive in the third dimension, that is, the thickness. The fact that the sheet resistance is thickness-independent confirms the confinement of the electrical charge transport in two dimensions, which is observed in polycrystalline metal oxide thin films. The temperature effect above 380 K indicates a transition from a two-dimensional (2D) toward a three-dimensional conduction (results not shown.) The temperature of this transition decreased with increasing film thickness and extrapolates to $T_{transition} = 300$ K with a film thickness of 150 nm. Therefore, films with thicknesses higher than 150 nm no longer present this 2D confinement above room temperature.

The observed 2D confinement of the charge transport agrees with the presence of a surface-related ferromagnetism at low temperature.[19-21] This effect was attributed to the surface cobalt coordination that stabilizes the higher spin states of cobalt within a few unit cells at the surface. This configuration leads to a surface concentration of Co^{4+} cations that are also the charge carriers (holes), which largely exceeds that of the bulk $LaCoO_3$ single crystal.[21] Because of this charge carriers' abundance at the surface, the bulk contribution to the electrical conduction is negligible in ultrathin films. Nevertheless, with increased thickness, the contribution of the surface remains constant, whereas that of the bulk increases. As a consequence, for a constant temperature, there is a threshold thickness above which the 2D confinement of the charge transport vanishes, as observed in this study.

The investigation of the electrical behavior before and after a partial desorption of oxygen was performed with the objective to provide experimental evidence on the involvement of the adsorbed oxygen in the 2D confinement of the charge transport. The obtained results for 35 and 64 nm thick films are depicted in Fig. 5. As can be noticed in Fig. 4, Fig. 5 shows that the 35 and 64 nm thick films exhibit the same sheet resistance in the investigated temperature range under air atmosphere, which is an indication of the 2D confinement of the charge transport. The partial removal of the adsorbed oxygen species was achieved by a 30 min heat-treatment at 350°C under argon atmosphere, and a subsequent measurement of the electrical conductivity was performed under the same atmosphere at a pressure of 1 atm. This treatment's temperature was selected below the deposition temperature to avoid any sintering effect. The partial desorption of oxygen (Fig. 5) leads to a substantial increase in the sheet resistance, which also became thickness-dependent. As a consequence, the expected higher resistance for thinner films is re-

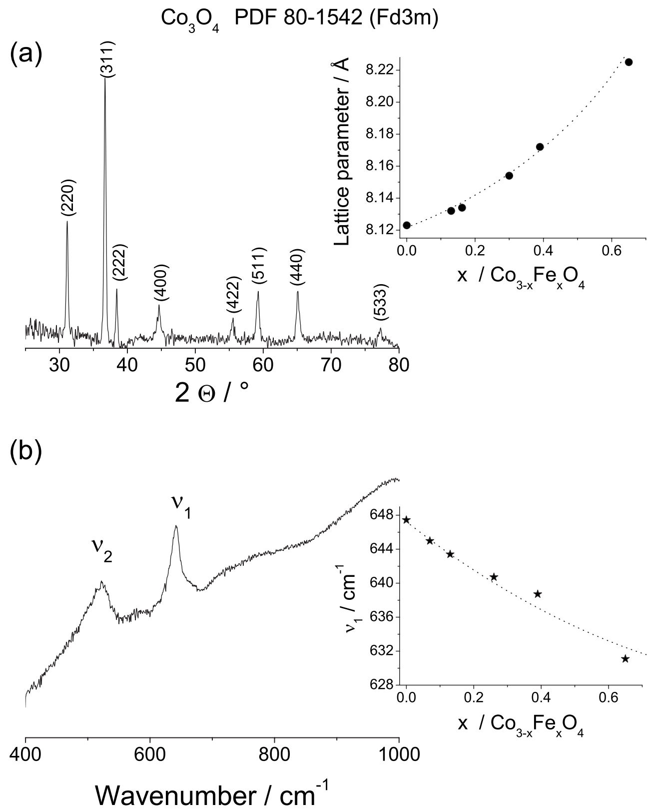

Figure 6. (a) Identification of the spinel structure of cobalt oxide by XRD and (b) FTIR emission spectroscopy, and the effect of iron insertion on the variation of the lattice parameter as calculated from the XRD data [insert in (a)] and on the vibration frequency of the characteristic bands [insert in (b)].

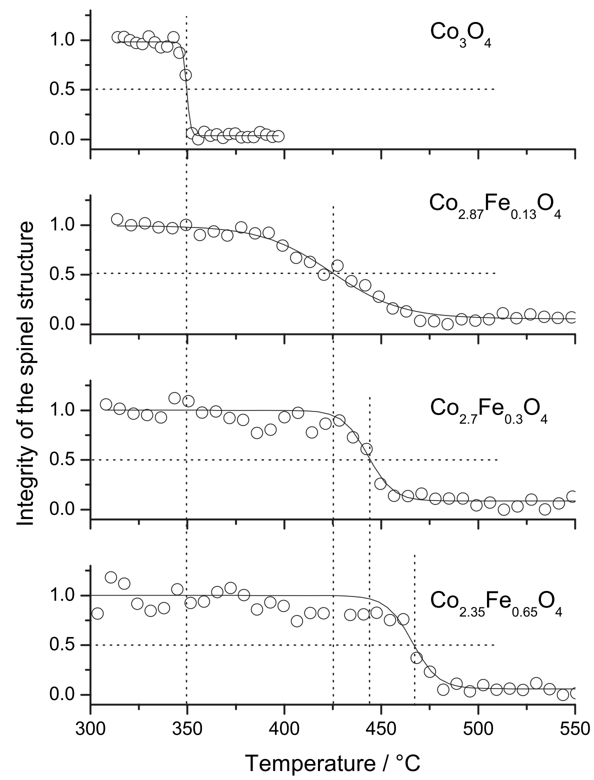

Figure 7. The effect of iron content on the temperature-programmed reduction profile of cobalt oxide: The integrity of the spinel structure was estimated by the monitoring of the area under the emission band ν_1 as a function of the temperature.

trieved. These indications clearly demonstrate the collapse of the 2D confinement. Therefore, these results provide experimental evidence regarding the involvement of the adsorbed oxygen in the confinement of the charge transport at the surface of ultrathin films of polycrystalline perovskite oxide, which holds significant potential in terms of technological applications.

Tuning the composition, properties, and reactivity of spinel oxide.— The material investigated here is cobalt oxide, which crystallizes in the normal spinel structure with divalent cobalt in the tetrahedral sites and trivalent cobalt in the octahedral sites. The possibility of tuning the properties and the reactivity of the normal spinel of cobalt oxide was investigated using iron as a doping element.

The normal spinel of cobalt oxide was grown with CVD at a substrate temperature of 500°C. Figure 6 shows the XRD pattern and the IR emission signature of the obtained polycrystalline Co_3O_4 films. Introducing iron into the lattice of the spinel was illustrated by the increased lattice parameter and the shift in the characteristic vibrational bands.

Consequent modifications of the electrical and redox properties of the spinel have been induced upon the insertion of iron into the lattice. The room temperature electrical conductivity shows an exponential decay with iron content from 10 Ω cm for pure cobalt oxide to 0.08 Ω cm with $Co_{3-x}Fe_xO_4$, $x = 0.65$. The reducibility of the spinel structure to the monoxide phase was investigated in an atmosphere of argon containing 5 vol % of hydrogen upon a temperature increase with a ramp of 6°C/min. The reaction monitoring was performed using the FTIR emission spectroscopy, and the results are presented in Fig. 7. The incorporation of iron into the spinel structure was shown to systematically shift the reduction to higher temperatures. The highly doped spinel, $x = 0.65$, was reduced at 465°C, while pure cobalt oxide is already reduced at 350°C.

The reactivity of the iron-doped spinel was investigated for the combustion of CO and ethanol in diluted air flow. As depicted in Fig. 8, contrasting behaviors were observed for CO and ethanol oxidation, which is an indication of the involvement of distinct active sites. The efficiency of the spinel catalyst toward the oxidation of CO correlates with the redox properties of the spinel. Increasing the amount of iron doping lowers the catalyst efficiency and shifts the onset to higher temperatures. This correlation agrees with the involvement of the reduction or the reoxidation of the catalyst as a rate-limiting step, which corresponds to the Mars–van Krevelen mechanism. This conclusion is in line with the isotope labeling experiments performed for pure cobalt oxide.[22]

The catalytic oxidation of ethanol over $Co_{3-x}Fe_xO_4$ proceeds by a partial oxidation to acetaldehyde at low temperatures, whereas CO_2 forms as a final product at high temperatures. The reactivity of the spinel toward the oxidation of ethanol was enhanced by the incorporation of iron into the lattice of Co_3O_4, as shown in Fig. 8. Previous reports on the ethanol oxidation over a manganese oxide catalyst have established a correlation between the catalyst efficiency and the presence of Mn^{3+}–Mn^{4+} couples.[23,24] The existence of tetravalent cations in the studied cobalt-oxide-based spinel can be associated with the electrical conductivity that occurs via the transport of holes (tetravalent cations). The enhanced presence of tetravalent cations with increased iron doping is assumed to favor the oxygen adsorption forming surface basic sites. These sites were reported to be responsible for the conversion of ethanol to acetaldehyde.[25]

Conclusions

The growth of various perovskites has been demonstrated using CVD, and the resulting films show properties that are comparable to the corresponding bulk material already at a thickness of 250 nm. The growth of ultrathin coalescent films, however, has enabled the observation of an intriguing property. Ultrathin films were shown to

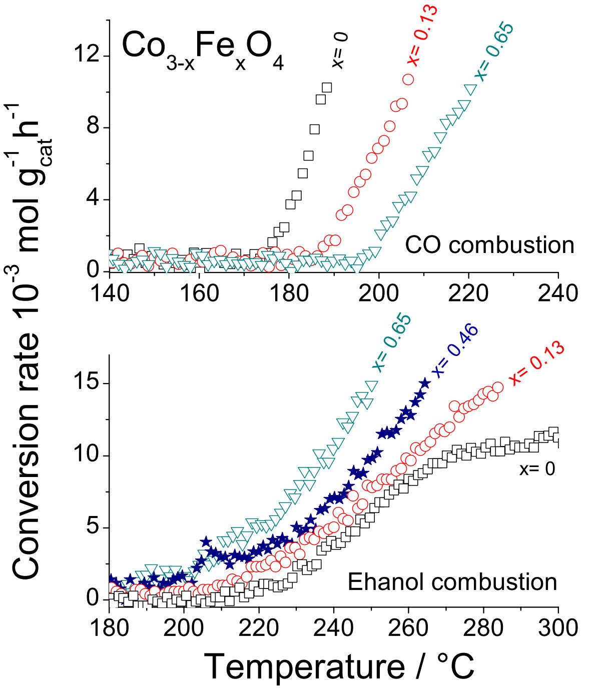

Figure 8. (Color online) Oxidative conversion of CO and ethanol over iron-doped spinel. The contents of CO and ethanol in the inlet air flow were 650 and 1000 ppm, respectively, and the space velocity was ~660 L g_{cat}^{-1} h^{-1} in both cases.

almost exclusively transport electricity at their surfaces. The observation of this 2D confinement of the charge transport was enabled by the possibility to grow coalescent polycrystalline ultrathin films of $LaCoO_3$.

Doping was used as a strategy for the modification of the physicochemical properties of the Co_3O_4 spinel and therefore its reactivity. Iron doping, which hinders the reducibility of the spinel, was found to lower the catalytic efficiency toward CO oxidation, which is an indication that the catalytic reaction takes place via the Mars–van Krevelen mechanism. Iron doping has also increased the electrical conductivity of the spinel, which means that tetravalent cations and charge carriers are more available in the lattice. The consequence of this effect is the increased ability of the catalyst to adsorb oxygen, which forms basic sites and enhances the catalytic oxidative conversion of ethanol.

Acknowledgments

One of the authors (P.H.T.N.) thanks Deutscher Akademischer Austausch Dienst for his fellowship grant at the University of Bielefeld in Germany.

University of Bielefeld assisted in meeting the publication costs of this article.

References

1. M. B. Salamon and M. Jaime, *Rev. Mod. Phys.*, **73**, 583 (2001).
2. P. A. Lee, N. Nagaosa, and X. G. Wen, *Rev. Mod. Phys.*, **78**, 17 (2006).
3. R. Ramesh and D. G. Schlom, *MRS Bull.*, **33**, 1006 (2008).
4. H. Zheng, J. Wang, S. E. Lofland, Z. Ma, L. Mohaddes-Ardabili, T. Zhao, L. Salamanca-Riba, S. R. Shinde, S. B. Ogale, F. Bai, et al., *Science*, **303**, 661 (2004).
5. R. Ramesh and N. A. Spaldin, *Nature Mater.*, **6**, 21 (2007).
6. Y. Bai, C. Knittlmayer, S. Gledhill, I. Lauermann, C. H. Fischer, and W. Weppner, *Ionics*, **15**, 11 (2009).
7. X. M. Chen, G. H. Wu, P. Jiang, W. F. Liu, and D. H. Bao, *Appl. Phys. Lett.*, **94**, 033501 (2009).
8. T. A. S. Ferreira, J. C. Waerenborgh, M. H. R. M. Mendonca, M. R. Nunes, and F. M. Costa, *Solid State Sci.*, **5**, 383 (2003).
9. V. A. Khomchenko, D. A. Kiselev, M. Kopcewicz, M. Maglione, V. V. Shvartsman, P. Borisov, W. Kleemann, A. M. L. Lopes, Y. G. Pogorelov, J. P. Araujo, et al., *J. Magn. Magn. Mater.*, **321**, 1692 (2009).
10. S. Bhattacharjee, E. Bousquet, and P. Ghosez, *Phys. Rev. Lett.*, **102**, 117602 (2009).
11. A. Ohtomo and H. Y. Hwang, *Nature (London)*, **427**, 423 (2004).
12. M. P. Warusawithana, C. Cen, C. R. Sleasman, J. C. Woicik, Y. L. Li, L. F. Kourkoutis, J. A. Klug, H. Li, P. Ryan, L. P. Wang, et al., *Science*, **324**, 367 (2009).
13. A. A. Bosak, C. Dubourdieu, P. Chaudouet, J. P. Senateur, and T. Fournier, *J. Appl. Phys.*, **94**, 5021 (2003).
14. Y. Rozier, B. Gautier, G. Hyvert, A. Descamps, C. Plossu, C. Dubourdieu, and F. Ducroquet, *Thin Solid Films*, **517**, 1868 (2009).
15. N. Bahlawane, P. A. Premkumar, J. Feldmann, and K. Kohse-Hoinghaus, *Chem. Vap. Deposition*, **13**, 118 (2007).
16. P. H. T. Ngamou and N. Bahlawane, *J. Solid State Chem.*, **182**, 849 (2009).
17. Y. Kobayashi, T. Nakajima, and K. Asai, *J. Magn. Magn. Mater.*, **272**, 83 (2004).
18. Y. Tokura, Y. Okimoto, S. Yamaguchi, H. Taniguchi, T. Kimura, and H. Takagi, *Phys. Rev. B*, **58**, R1699 (1998).
19. J. Q. Yan, J. S. Zhou, and J. B. Goodenough, *Phys. Rev. B*, **70**, 014402 (2004).
20. S. M. Zhou, L. Shi, J. Y. Zhao, L. F. He, H. P. Yang, and S. M. Zhang, *Phys. Rev. B*, **76**, 172407 (2007).
21. A. Harada, T. Taniyama, Y. Takeuchi, T. Sato, T. Kyomen, and M. Itoh, *Phys. Rev. B*, **75**, 184426 (2007).
22. J. Jansson, *J. Catal.*, **194**, 55 (2000).
23. S. J. A. Figueroa, F. G. Requejo, E. J. Lede, L. Lamaita, M. A. Peluso, and J. E. Sambeth, *Catal. Today*, **107–108**, 849 (2005).
24. L. Lamaita, M. A. Peluso, J. E. Sambeth, and H. J. Thomas, *Appl. Catal., B*, **61**, 114 (2005).
25. B. Bialobok, J. Trawczynski, W. Mista, and M. Zawadzki, *Appl. Catal., B*, **72**, 395 (2007).